The Astrophysical Journal Letters, 907:L20 (9pp), 2021 January 20 https://doi.org/10.3847/2041-8213/abd4d3
© 2021. The Author(s). Published by the American Astronomical Society.
OPEN ACCESS

Eccentric Black Hole Mergers in Active Galactic Nuclei

Hiromichi Tagawa[1], Bence Kocsis[2], Zoltán Haiman[3], Imre Bartos[4], Kazuyuki Omukai[1], and Johan Samsing[5]
[1] Astronomical Institute, Graduate School of Science, Tohoku University, Aoba, Sendai 980-8578, Japan; htagawa@astr.tohoku.ac.jp
[2] Rudolf Peierls Centre for Theoretical Physics, Clarendon Laboratory, Parks Road, Oxford, OX1 3PU, UK
[3] Department of Astronomy, Columbia University, 550 W. 120th St., New York, NY, 10027, USA
[4] Department of Physics, University of Florida, PO Box 118440, Gainesville, FL 32611, USA
[5] Niels Bohr International Academy, The Niels Bohr Institute, Blegdamsvej 17, 2100 Copenhagen, Denmark
Received 2020 October 20; revised 2020 December 9; accepted 2020 December 17; published 2021 January 21

Abstract

The astrophysical origin of gravitational wave transients is a timely open question in the wake of discoveries by the Laser Interferometer Gravitational-Wave Observatory (LIGO)/Virgo. In active galactic nuclei (AGNs), binaries form and evolve efficiently by interaction with a dense population of stars and the gaseous AGN disk. Previous studies have shown that stellar-mass black hole (BH) mergers in such environments can explain the merger rate and the number of suspected hierarchical mergers observed by LIGO/Virgo. The binary eccentricity distribution can provide further information to distinguish between astrophysical models. Here we derive the eccentricity distribution of BH mergers in AGN disks. We find that eccentricity is mainly due to binary–single (BS) interactions, which lead to most BH mergers in AGN disks having a significant eccentricity at 0.01 Hz, detectable by the Laser Interferometer Space Antenna. If BS interactions occur in isotropic-3D directions, then 8%–30% of the mergers in AGN disks will have eccentricities at 10 Hz above $e_{10\,\mathrm{Hz}} \gtrsim 0.03$, detectable by LIGO/Virgo/Kamioka Gravitational Wave Detector, while 5%–17% of mergers have $e_{10\,\mathrm{Hz}} \geqslant 0.3$. On the other hand, if BS interactions are confined to the AGN–disk plane due to torques from the disk, with 1–20 intermediate binary states during each interaction, or if BHs can migrate to $\lesssim 10^{-3}$ pc from the central supermassive BH, then 10%–70% of the mergers will be highly eccentric ($e_{10\,\mathrm{Hz}} \geqslant 0.3$), consistent with the possible high eccentricity in GW190521.

Unified Astronomy Thesaurus concepts: Active galactic nuclei (16); Gravitational wave sources (677); Close binary stars (254); N-body simulations (1083); Stellar mass black holes (1611)

1. Introduction

Recent detections of gravitational waves (GWs) have shown evidence for a high black hole (BH) merger rate in the universe (Abbott et al. 2019b). However, the proposed astrophysical pathways to merger remain debated.

Measuring the binary eccentricity (e) is useful to distinguish between possible astrophysical pathways to merger. The feasibility to measure e has increased tremendously due to the improvement of the detectors and GW data analysis methods (e.g., Nishizawa et al. 2016; Lower et al. 2018; Abbott et al. 2019a; Romero-Shaw et al. 2019). At design sensitivity, the Laser Interferometer Gravitational-Wave Observatory (LIGO), Virgo, and Kamioka Gravitational Wave Detector (KAGRA) detectors may detect eccentricities at 10 Hz above $e_{10\mathrm{Hz}} \gtrsim 0.03$ (Lower et al. 2018; Gondán & Kocsis 2019; Romero-Shaw et al. 2019), while Laser Interferometer Space Antenna (LISA) will detect e if above 10^{-3}–10^{-2} at 0.01 Hz (Nishizawa et al. 2016). Eccentricity varies greatly among different merger channels (Antonini & Perets 2012; Breivik et al. 2016; Antonini et al. 2017; Silsbee & Tremaine 2017; Arca-Sedda et al. 2018; Samsing & D'Orazio 2018; Rodriguez et al. 2018; Fragione et al. 2019; Fragione & Bromberg 2019; Zevin et al. 2019; Martinez et al. 2020), but only binaries formed through GW capture (GWC) are generally expected to produce mergers with $e_{10\mathrm{Hz}} \gtrsim 0.1$ (Kocsis et al. 2006; O'Leary et al. 2009; Gondán et al. 2018; Samsing 2018; Rasskazov & Kocsis 2019; Gondán & Kocsis 2020).

Original content from this work may be used under the terms of the Creative Commons Attribution 4.0 licence. Any further distribution of this work must maintain attribution to the author(s) and the title of the work, journal citation and DOI.

Recently, the merger of two unusually heavy BHs, GW190521, was reported (Abbott et al. 2020a; Abbott et al. 2020b). Their high masses ($85^{+21}_{-21}\,M_\odot$ and $66^{+17}_{-18}\,M_\odot$) and high spins ($0.69^{+0.27}_{-0.62}$ and $0.73^{+0.24}_{-0.64}$) indicate that the merging BHs themselves could have been the remnants of earlier BH mergers, which increased their masses beyond the $\sim 56\,M_\odot$ limit due to pulsational pair-instability (Farmer et al. 2019) and their spins beyond the small natal values expected in stellar evolutionary models of angular momentum transfer (Fuller & Ma 2019). Thus, detection of GW190521 (and also other events: GW170729, GW170817A, GW190412, and GW190814; Zackay et al. 2019; Abbott et al. 2020c, 2020d) suggests that hierarchical mergers could be frequent among compact objects. This is consistent with the scenario of mergers in active galactic nucleus (AGN) disks (e.g., Yang et al. 2019, 2020; Tagawa et al. 2020a, hereafter Paper II), in which binaries are efficiently hardened by interaction with the surrounding gas (e.g., Bartos et al. 2017; Stone et al. 2017; McKernan et al. 2018) and with the dense populations of stars and compact objects (Tagawa et al. 2020b, hereafter Paper I). A possible electromagnetic counterpart would further support this scenario (McKernan et al. 2019; Graham et al. 2020).

Interestingly, Gayathri et al. (2020) found that GW190521 prefers a high eccentricity of $e_{10\mathrm{Hz}} \sim 0.7$, along with high spin-precession (see also Romero-Shaw et al. 2020). A high eccentricity places additional constraints on possible astrophysical models of this source (e.g., Zevin et al. 2019; Rodriguez et al. 2018; Rasskazov & Kocsis 2019).

Samsing et al. (2020a) recently showed that highly eccentric mergers are common in AGN disks by assuming that binary–single (BS) interactions of BHs are confined to a plane. That study assumed constant values for the frequency of BS interactions,

initial separation, and relative velocity of a third body based on Paper I. In this Letter, we investigate the distribution of the binary eccentricity for mergers in AGN disks by performing 1D N-body simulations combined with semi-analytical prescriptions, which enable us to follow binaries considering such effects as eccentricity evolution due to BS interactions, type I/II torques exerted by circumbinary disks, and GW radiation (Section 2.3). We also augment the model used in Paper I/Paper II to include GW capture in single–single (SS) and BS encounters.

2. Method

Our model is based on that in Paper I and partially in Paper II as specified below. The new ingredients are described in some detail in Sections 2.2.1, 2.3.2, and 2.4.

2.1. Components

We suppose that there is a supermassive BH (SMBH) at the center of a galaxy and it has a gaseous accretion disk (hereafter "AGN disk") and a spherically distributed stellar cluster (hereafter "spherical component"). We follow the evolution of the BH system consisting of a cluster of BHs around the AGN disk (called the flattened component due to its spatial distribution, which is assumed to be caused by vector resonant relaxation; Szolgyen & Kocsis 2018), and stars and BHs captured inside the AGN disk due to the gaseous torque (called the disk stellar/BH components). See Figure 1 in Paper I for an illustration of these components.

2.2. Binary Formation and Disruption

Some BHs in the flattened component are in binaries from the outset (called pre-existing binaries). In the AGN disk, binaries form due to gas dynamical friction during two-body encounters (dubbed the gas-capture binary formation). Binaries also form due to dynamical interactions during three-body encounters (dynamical binary formation). At their formation, a thermal distribution $f(e)=2e$ is assumed, while $e=0$ was assumed in Paper I/Paper II. In addition to those mechanisms already included in Paper I, we here consider the binaries formed by the GWC mechanism (e.g., O'Leary et al. 2009; Samsing et al. 2020b), which are relevant for highly eccentric mergers, as described below in Section 2.2.1. Binaries are disrupted by soft-BS interactions, in which the binaries become softer (e.g., Heggie 1975).

2.2.1. Binary Formation by the GW Capture

We treat binary formation by GWC due to SS encounters (SS–GWC) and BS interactions (BS–GWC) separately as described below.

In an SS encounter event, a binary can form if the two bodies approach close enough that the energy radiated by GWs ($\Delta E_{\rm GW}$) exceeds their kinetic energy, $E_{\rm SS}\approx \frac{1}{2}\mu v_{12}^2$, where μ is the reduced mass, and v_{12} the relative velocity. $\Delta E_{\rm GW}$ is approximately given as

$$\Delta E_{\rm GW}\approx \frac{85\pi}{12\sqrt{2}}\frac{G^{7/2}\eta^2 m_{\rm tot}^{9/2}}{c^5 r_{\rm p}^{7/2}}, \tag{1}$$

(e.g., O'Leary et al. 2009), where G is the gravitational constant, c the light speed, $m_{\rm tot}$ the total mass of the two bodies, η the symmetric mass ratio, and the pericenter distance

$$r_{\rm p}=\left(\sqrt{\frac{1}{b^2}+\frac{G^2 m_{\rm tot}^2}{b^4 v_{12}^4}}+\frac{G m_{\rm tot}}{b^2 v_{12}^2}\right)^{-1} \tag{2}$$

where b is the impact parameter of the encounter. By equating $\Delta E_{\rm GW}$ in Equation (1) and $E_{\rm SS}$, the maximum pericenter distance for the GWC is

$$r_{\rm p,max}=\left(\frac{85\pi\eta c^2}{6\sqrt{2}v_{12}^2}\right)^{2/7}\frac{G m_{\rm tot}}{c^2}. \tag{3}$$

Note that the gas has negligible impact on the dynamics during the GWC owing to very short timescale for the capture ($\sim$an hr; O'Leary et al. 2009). Here we define the maximum impact parameter $b_{\rm max}$ at which $r_{\rm p}=r_{\rm p,max}$. We assume that the cross section of SS–GWC $\sigma_{\rm SS}$ is approximately given as $\sigma_{\rm SS}=r_{\rm SS}z_{\rm SS}$, where $r_{\rm SS}=\min[b_{\rm max}, r_{\rm Hill}]$, $z_{\rm SS}=\min[r_{\rm SS}, h_{\rm c}]$, $r_{\rm Hill}=r(m_{\rm BH}/3M_{\rm SMBH})^{1/3}$ is the Hill radius with respect to the SMBH, $m_{\rm BH}$ is the mass of the BH, and $h_{\rm c}$ is the average orbital height of background objects at the radial location of the BH (see Paper I).

For each object, the timescale to undergo the SS–GWC is $t_{\rm GSS}=1/(n_{\rm c}\sigma_{\rm SS}v_{\rm rel})$, where $n_{\rm c}$ is the number density of background objects, and $v_{\rm rel}$ the typical relative velocity between the BH and background objects (Paper I). Here we substitute $v_{\rm rel}=v_{12}$ in Equations (1)–(2). We set the probability of binary formation by this mechanism during the timestep Δt to $P_{\rm GSS}=\Delta t/t_{\rm GSS}$. When the SS–GWC binaries form, we choose b so that b^2 is uniformly distributed between 0 and $b_{\rm max}^2$. The semimajor axis and e of the newly formed binary are $s=Gm_{\rm tot}^2\eta/(2|\Delta E_{\rm GW}|-2E_{\rm SS})$, and $e=1-r_{\rm p}/s$, respectively. We only consider binary formation through SS–GWC between disk BHs, as the probability of interactions is much lower for spherical component objects due to their large $v_{\rm rel}$ ($P_{\rm SS}\propto v_{\rm rel}^{-11/7}$ for $b_{\rm max}<h_{\rm c}$, $r_{\rm Hill}$), and due to the large physical sizes of stars. For binaries formed in this process, we assume that the orbital angular momentum directions are aligned (or half anti-aligned) with the angular momentum direction of the AGN disk.

GWC binaries can also form during BS interactions (e.g., Samsing et al. 2014) if one body is captured due to strong GW emission. Before the interaction, the velocities among BHs in the flattened component are likely distributed almost randomly in 3D space, while for interactions among the disk BHs the three-body velocities may be constrained in the AGN–disk plane due to the disk gas drag. We here study the 3D and 2D hard-BS interactions separately. In the case of the 3D hard-BS interactions, the probability of GWC binary formation is roughly given by

$$P_{\rm GBS}\simeq N_{\rm int}\frac{2r_{\rm p,max}}{s} \tag{4}$$

(Samsing 2018), where $N_{\rm int}$ is the average number of quasi-stable states for temporary binary BHs formed during a BS interaction, where $N_{\rm int}\sim 20$ is numerically verified for both 2D and 3D interactions in equal-mass cases (Samsing et al. 2014; Samsing et al. 2020a). The GWC probability is calculated as

$$P_{\rm GBS}=1-(1-P_{\rm GBS,1})^{N_{\rm int}} \tag{5}$$

where

$$P_{\rm GBS,1}=\frac{\int_{e_{\rm cr}}^{1}f(e)de}{\int_{0}^{1}f(e)de} \quad (6)$$

is the probability that GWC occurs in one interaction, $e_{\rm cr}=1-r_{\rm p,max}/s$ is the critical eccentricity above which the GWC binaries form due to GW emission, and $f(e)$ is either $f_{\rm 3D}=2e$ (e.g., Heggie 1975) or $f_{\rm 2D}=e/\sqrt{1-e^2}$ (Valtonen & Karttunen 2006) for isotropic-3D and 2D interactions, respectively.

When the BS interaction ends in a GW-capture, the semimajor axis s does not change from that before the BS interaction, we determine $r_{\rm p}=s(1-e)$ by drawing e from $f(e)$. This assumption is due to energy conservation, since in this case the third body does not receive a strong velocity kick and it is not ejected. Capture occurs only if $r_{\rm p}<r_{\rm p,max}$ (Equation (3)). We assume that $v_{12}=\sqrt{Gm_{\rm tot}/s}$, i.e., the intrinsic orbital velocity of the binary. For simplicity, we also assume that the BS–GWC results in binary formation among the most and second-most massive objects. Although a BS–GW-capture binary may be bound to the third object if the GW kick is small (Samsing & Ilan 2019), we ignore the third body after the binary formation for simplicity.

2.3. Evolution of Binary Separation, Mass, etc.

2.3.1. Gaseous Processes

The velocity of BHs relative to the local motion of the AGN disk decreases due to the accretion torque and gas dynamical friction. The semimajor axis (s) evolves due to gas dynamical friction by the AGN disk and type I/II migration torques exerted by a compact circumbinary disk that forms within the Hill sphere of the binary. The radial distances of BHs from the SMBH (r) are also allowed to evolve due to type I/II torques from the AGN disk. Gas accretion affects BH masses, BH spins, and the orbital angular momentum directions of binaries (Paper II). When gaps form around BHs, we assume that migration torques, gas dynamical friction, and gas accretion are weakened. Objects usually accumulate in gap-forming regions (Paper I), which act like migration traps.

2.3.2. Dynamical Processes

We also account for dynamical interactions with single stars/BHs and BH binaries in a way similar to the Monte-Carlo method (Paper I). The binaries' semimajor axes, velocities, and orbital angular momentum directions evolve due to BS interactions, and the velocities of all BHs additionally evolve due to scattering. In particular, the binary separation decreases during hard BS interactions, and the single object and the binary receive a recoil kick. When the interactions are confined in 2D, kicks are also assigned within the AGN–disk plane.

While binary component exchanges were neglected during BS interactions in Paper I/Paper II, here we assume that the components are always replaced by the most massive pair during hard-BS interactions, in which the binary becomes harder. During an exchange, the binary's binding energy is assumed to be unchanged (Sigurdsson & Phinney 1993). See the Appendix for the impact of including these exchange interactions. In binary–binary interactions, we assume that the binary composed of the two most massive objects experiences two BS interactions with the two less massive objects, which become unbound after the interaction.

2.3.3. Merger Prescription

Once binaries become sufficiently tight, their separation shrinks promptly by GW emission. We assume that the BHs merge when their pericenter distance becomes smaller than the innermost stable circular orbit, and then assign a kick velocity and mass loss due to the GW emission and prescribe BH spin evolution at the merger as in Paper I.

2.4. Binary Eccentricity Evolution

After formation, the binary eccentricity e changes due to GW emission, the torque by the circumbinary disk, and BS interactions. Below we describe our prescriptions for calculating those processes, which are newly incorporated in our model.

For the GW emission, we follow Peters (1964) to track the change of the eccentricity.

For the torque by the circumbinary disk, we use the fitting function of Equation (2) of Zrake et al. (2020) in $e\leqslant 0.8$ and assume $de/d\log m_{\rm bin}=-2.3$ in $e>0.8$. Their results using 2D hydrodynamical simulations suggest disks drive binaries to $e\approx 0.45$ (see also Muñoz et al. 2019).

During hard-BS interactions, we draw e randomly from $f(e)$ (see below Equation (6)). In the fiducial model, we assume that e follows $f_{\rm 3D}(e)$ after all hard-BS interactions, but see different choices in the Appendix.

2.5. Models Examined

The fiducial model parameters (M1) are listed in Table 1, which are the same as those in Paper I/Paper II. We also study the additional models M2–M4, which differ in the treatment of the BS interactions. While 3D BS interactions are assumed in model M1, motions of the three bodies may be confined to the AGN–disk plane before the interaction. Even in the latter case, the motion may be isotropized in 3D during the interaction by small perturbations, such as inhomogeneities/warps of the AGN disk and presence of other objects. To mimic such $2\rightarrow 3$D interactions, we examine another model (M2) in which the capture probability during a BS interaction is given by Equation (5) assuming that $N_{\rm int}=20$ 2D interactions take place with $f_{\rm 2D}(e)$. If a GW capture does not take place, the e distribution is drawn from $f_{\rm 3D}(e)$ and the binary angular momentum direction is randomized due to 3D interactions in later phases. We neglect the chance for GWC after interactions are randomized to 3D as its probability is much lower than that during 2D interactions. The reason to adopt the model with $2\rightarrow 3$D BS interactions instead of 2D BS interactions is stated in the Appendix. To assess the importance of BS interactions, we omit it altogether in model M3. Similar to model M3 but more realistic is model M4, in which BS interactions are made inefficient by reducing the initial BH number ($N_{\rm BH,ini}=6\times 10^3$) and enhancing the initial BH velocity dispersion ($\beta_{\rm v}=1$).

In models M1–M3, the initial number of BHs (binaries) is 2×10^4 (1.5×10^3), while in model M4 they are 6×10^3 (4.5×10^2). We present the results at 10 Myr.

3. Results

In Figure 1, we show the eccentricity distribution of mergers and the contribution of individual binary formation channels to

Table 1
Fiducial Values of Our Model Parameters

Parameter	Fiducial Value
Spatial directions in which BS interactions occur	isotropic in 3D
Number of temporary binary BHs formed during a BS interaction	$N_{\rm int}=20$
Initial BH spin magnitude	$\vert\boldsymbol{a}\vert=0$
Angular momentum directions of circum-BH disks	$\hat{\boldsymbol{J}}_{\rm CBHD}=\hat{\boldsymbol{J}}_{\rm AGN}$ for single BHs, $\hat{\boldsymbol{J}}_{\rm CBHD}=\hat{\boldsymbol{J}}_{\rm bin}$ for BHs in binaries
Ratio of viscosity responsible for warp propagation over that for transferring angular momentum	$\nu_2/\nu_1=10$
Alignment efficiency of the binary orbital angular momentum due to gas capture (Equation (14) in Paper II)	$f_{\rm rot}=1$
Mass of the central SMBH	$M_{\rm SMBH}=4\times10^6\,M_\odot$
Gas accretion rate at the outer radius of the simulation (5 pc)	$\dot{M}_{\rm out}=0.1\,\dot{M}_{\rm Edd}$ with $\eta=0.1$
Fraction of pre-existing binaries	$f_{\rm pre}=0.15$
Power-law exponent for the initial density profile for BHs	$\gamma_\rho=0$
Initial velocity anisotropy parameter such that $\beta_{\rm v}v_{\rm kep}(r)$ is the BH velocity dispersion	$\beta_{\rm v}=0.2$
Efficiency of angular momentum transport in the α-disk	$\alpha_{\rm SS}=0.1$
Stellar mass within 3 pc	$M_{\rm star,3pc}=10^7\,M_\odot$
Stellar initial mass function slope (relation between the stellar and BH masses are in Equation (3) of Paper I)	$\delta_{\rm IMF}=2.35$
Angular momentum transfer parameter in the outer star-forming regions (Equation C8 in Thompson et al. 2005)	$m_{\rm AM}=0.15$
Accretion rate in Eddington units onto stellar-mass BHs with a radiative efficiency $\eta=0.1$	$\Gamma_{\rm Edd,cir}=1$
Numerical timestep parameter	$\eta_t=0.1$
Number of radial cells storing physical quantities	$N_{\rm cell}=120$
Maximum and minimum r for the initial BH distribution	$r_{\rm in,BH}=10^{-4}$ pc, $r_{\rm out,BH}=3$ pc
Initial number of BHs within 3 pc	$N_{\rm BH,ini}=2\times10^4$

it. Figure 2 shows the expected distribution of the mass-weighted sum of the individual spin components perpendicular to the orbital plane $\chi_{\rm eff}$, the precession parameter $\chi_{\rm p}$ (top row), the primary mass m_1, and e (bottom row) of the observed mergers except for model M3. For M3, the $\chi_{\rm eff}$ and $\chi_{\rm p}$ distributions are not shown since $\chi_{\rm p}$ is always 0 due to the assumption that the orbital planes of SS–GWC binaries are aligned with the AGN–disk plane (Section 2.2.1). The merger rate is weighted by the detection volume in the same manner as in Paper I/Paper II and the eccentricity is calculated at the GW frequency of 10 Hz as in Equation (36) of Wen (2003).

In the fiducial model M1, where the BS interaction is assumed to be 3D, ∼14% of mergers have a significantly nonzero eccentricity ($e_{\rm 10Hz}\gtrsim0.03$) measurable by the current ground-based detectors LIGO/Virgo/KAGRA (e.g., Romero-Shaw et al. 2019, but see also Huerta & Brown 2013), due to GWC binary formation (Figure 1 and Table 2) and frequent BS interactions. While most AGN merger events take place among binaries of non-GWC origin, which have lower e (Figure 1(a)), LISA observations will be able to measure e as low as $e\gtrsim10^{-3}-10^{-2}$ at ∼0.01 Hz (e.g., Nishizawa et al. 2016), corresponding to $e_{\rm 10Hz}\gtrsim10^{-7}$ if binaries evolve only by GW emission. $e_{\rm 10Hz}$ are typically distributed in higher values (∼10^{-3}–10^{-2}) than those of mergers in globular clusters (∼10^{-7}–10^{-4}; Rodriguez et al. 2018) and isolated binaries (∼10^{-7}–10^{-6}; Breivik et al. 2016), while the similar values to those in triple system (∼10^{-3}–10^{-2}; Antonini et al. 2017).

Due to randomization of the orbital angular momentum direction by frequent BS interactions before mergers, $\chi_{\rm eff}$, and $\chi_{\rm p}$ tend to be distributed at low and high values (top row, Figure 2(a)), respectively. The physical properties, $\chi_{\rm eff}$, $\chi_{\rm p}$, and m_1 of GW190521 are generally consistent with the predictions by model M1, while the possible high e implied by Gayathri et al. (2020) is in tension with this model (bottom row, Figure 2(a)).

In model M2 with $2\rightarrow3$D BS interactions, the fraction of the BS–GWC binary mergers among the detectable events $f_{\rm GWBS}$ is elevated to 0.84 (from 0.10 of model M1; see Table 2), and they have very high eccentricity $e\gtrsim0.1$ (Figure 1(b)). In this way, BS interactions significantly increase the rate of highly eccentric mergers (see also Samsing et al. 2020a). The mass of GW190521, however, appears to be somewhat too high compared with the typical values in model M2 (bottom row, Figure 2(b)), but the model may still be consistent with the event as the mass distribution for high-e events has been poorly constrained.

In model M3, where the BS interaction is omitted, the (SS-)GWC binary mergers occupy a high fraction of $f_{\rm GWSS}=0.54$ favoring mergers between high-generation BHs (top row, Figure 2(c)). High-generation BHs are those that have already experienced mergers in the past, and they tend to have high eccentricities around $\gtrsim$0.1 (Figure 1(c)). Here, binary formation occurs mostly by the (SS-)GWC because BHs rapidly migrate without delay by kicks at the BS interactions to the inner AGN disk of $r\lesssim10^{-3}$ pc (e.g., Figure 1 of Paper II), where non-GW-capture channels by the gas-capture and dynamical binary formation are inefficient due to high shear velocity ($\gtrsim$tens km s^{-1}).

In general, the frequency of the SS–GWC $f_{\rm GWSS}$ increases as the initial BH number decreases (see the Appendix). For example, in model M4, where $N_{\rm ini}=6000$ and $\beta_{\rm v}=1$, $f_{\rm GWSS}$ becomes as high as 0.38. The prediction of positive $\chi_{\rm p}$, high e, and high-BH mass m_1 in this model agrees with the observed properties of GW190521 (Figure 2(d)). Although the number of mergers is smaller by a factor of ∼10 compared to that in the fiducial model, it is still consistent with the rate of GW190521-like events (see Section 5.5 of Paper I).

As seen above, the AGN origin can naturally reproduce the occurrence of GW190521-like mergers. In several models, the eccentricity distribution allows us to distinguish specific types of the GWC events (orange and red lines in Figure 1) due to

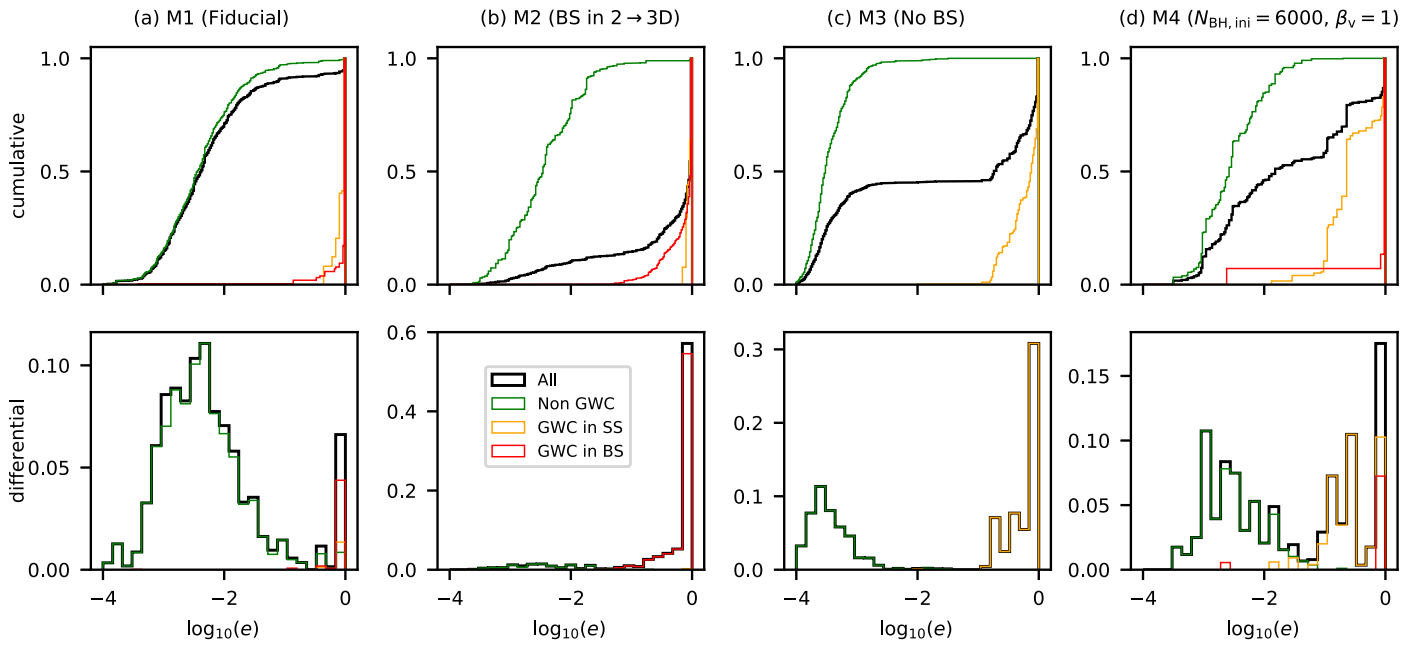

Figure 1. Cumulative (top row) and differential (bottom row) detection rate distributions of the eccentricity at 10 Hz $e_{\rm 10Hz}$ for models M1 (a), M2 (b) in which BS interactions occur in $2 \rightarrow 3$D space (Section 2.5), M3 (c) in which BS interaction does not operate, and M4 (d) in which the initial BH number is low ($N_{\rm ini}=6000$) and the initial velocity dispersion of BHs is high ($\beta_{\rm v}=1$). In addition to the sum of all binary mergers (black), separate contributions from binaries due to the non-GWC (green), SS–GWC (orange), and BS–GWC (red) are shown.

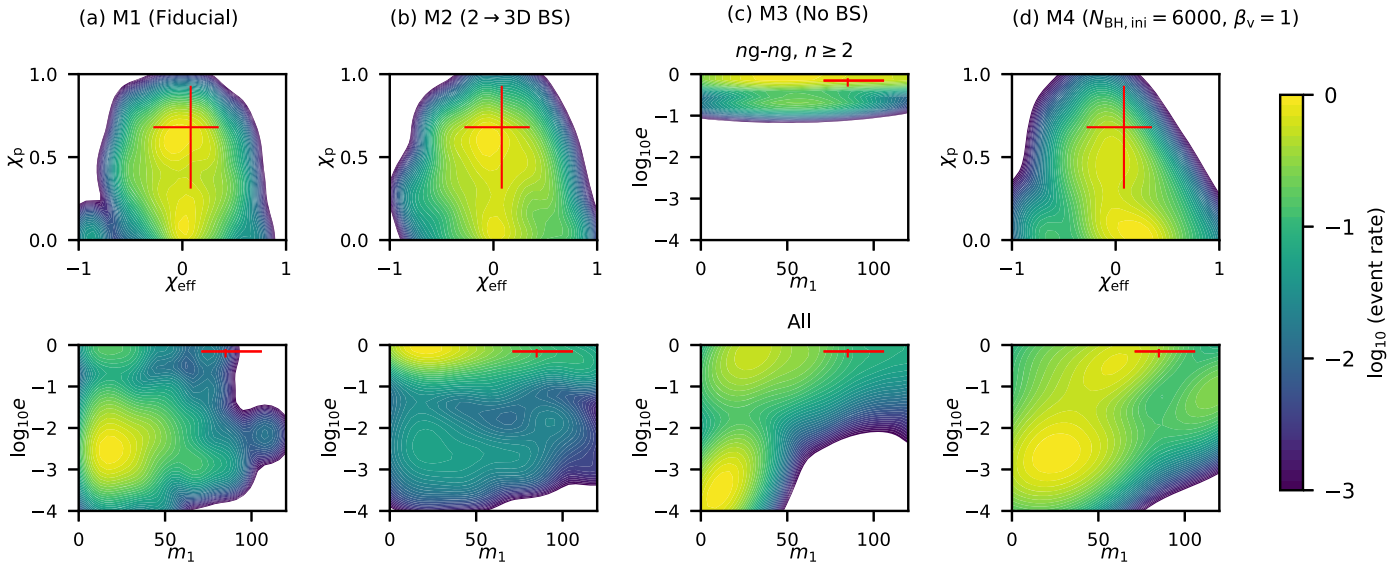

Figure 2. Detection rate distributions of several parameters for the same models as in Figure 1. The top and bottom rows show distributions of $\chi_{\rm eff}$–$\chi_{\rm p}$ and m_1–$\log_{10}$ $e_{\rm 10Hz}$, respectively, while in model M3, m_1–$\log_{10}$ $e_{\rm 10Hz}$ are shown for all mergers (bottom row) and mergers among n-generation ($n \geqslant 2$) BHs (top row). The error bars correspond to the 90 percentile credible intervals for GW190521 (Abbott et al. 2020a), while we here roughly assume $e_{\rm 10Hz}=0.7^{+0.1}_{-0.2}$, referring to Gayathri et al. (2020).

differences in the initial relative velocity involved (Equation (3)) and such high eccentricities are measurable by LIGO/Virgo/KAGRA. The consistency of other observables of GW190521 will be examined in a follow-up paper.

In the AGN channel, the SMBH helps retain recoiling merger remnants and allows multiple mergers among high-generation BHs, while the AGN disk helps to (1) deliver the single objects to the dense inner nucleus where the interactions are frequent, (2) form binaries through the process of gas-capture binary formation, and (3) contributes to reducing the binary separation at relatively large separations. The rate of GWC mergers and the eccentricity distribution are influenced by the frequency of interactions in addition to the prescription for BS interactions, while they are less affected by other processes as discussed in more detail in the Appendix.

4. Conclusions

In this Letter we have investigated the eccentricity distribution of merging BHs in AGN accretion disks. Our conclusions are summarized as follows.

Table 2
The Assumptions and Results in Different Models

Input		Output							
Model	Parameter	$f_{\rm noGWC}$	$f_{\rm GWSS}$	$f_{\rm GWBS}$	$f_{\rm e,0-003}$	$f_{\rm e,003-03}$	$f_{\rm e,03-09}$	$f_{\rm e,09-1}$	$N_{\rm mer}$
M1	Fiducial	0.93	0.02	0.05	0.86	0.065	0.022	0.057	1.1×10^{3}
M2	BS in $2\rightarrow3$D	0.14	3×10^{-3}	0.86	0.25	0.082	0.20	0.47	2.3×10^{3}
M3	No BS	0.46	0.54	0	0.46	0.092	0.26	0.19	9.0×10^{2}
M4	$N_{\rm BH,ini}=6000$, $\beta_{\rm v}=1$	0.55	0.38	0.078	0.54	0.27	0.048	0.15	1.3×10^{2}

Note. The input columns show the model number and the differences with respect to the fiducial model. "BS in $2\rightarrow3$D" represents the model in which BS interactions occur in $2\rightarrow3$D space (Section 2.5), "No BS" represents the model in which BS interactions do not operate. The output columns list the detection fraction of mergers among non-GWC binaries ($f_{\rm noGWC}$), GWC binaries formed in SS encounters ($f_{\rm GWSS}$), and those in BS interactions ($f_{\rm GWBS}$) with respect to all mergers, the detection fractions of mergers whose $e_{10\ \rm Hz}$ are in the range 0–0.03, 0.03–0.3, 0.3–0.9, and 0.9–1, respectively, and the number of mergers ($N_{\rm mer}$).

Table 3
Main Assumptions and Simplifications Made in Our Model

1	The AGN disk is in steady state and the SMBH is static.
2	The formation and evolution of compact objects and their binaries other than BHs are neglected.
3	Stable triple systems composed of stellar-mass BHs (e.g., Antonini et al. 2017) are not taken into account.
4	Massive perturbers (Deme et al. 2020) are not considered.
5	In the outer regions of the AGN disk, BHs form directly without experiencing stellar phases.
6	The AGN disk and the flattened BH component are initially rotating in the same direction.
7	Gas captured by BHs (binaries) rotates in the same direction to the AGN disk (Lubow et al. 1999) before viscous torques operate.
8	The most massive pair remains in a binary after hard BS interactions.
9	Softer binaries are always disrupted after hard binary–binary interactions.
10	Kick velocities at hard-BS interactions are given by a mode of their distribution referring to Leigh et al. (2018)

1. Due to frequent BS interactions in gap-forming regions of the AGN disk, eccentricities at 10 Hz are above $e_{\rm 10Hz}\geqslant10^{-4}$ for all stellar-mass BH mergers in AGNs in our models. LIGO together with LISA will be able to constrain the corresponding astrophysical models at high and low frequencies, respectively.
2. If BS interactions occur in isotropic-3D directions, ∼8%–30% of detectable mergers have $e_{\rm 10Hz}\gtrsim0.03$, i.e., above the value possibly measurable by LIGO/Virgo/KAGRA.
3. If BS interactions occur in 2D or $2\rightarrow3$D directions due to torques from the AGN disk, the mergers among GWC binaries formed during BS interactions become very frequent (∼15%–90%). Also, if BHs can migrate to $r\lesssim10^{-3}$ pc due to low BH density in the AGN disk, those formed in SS encounters are significantly enhanced (∼40%–70%). In these cases, ∼10%–70% of detectable mergers have $e_{\rm 10Hz}\geqslant0.3$, which may explain the possible extreme eccentricity implied for GW190521 by Gayathri et al. (2020).

We have neglected the evolution of e by soft-BS interactions, weak scattering, and gas dynamical friction, which presumably have minor effects on e as their contributions on the later evolution of binaries are negligibly small. However, hierarchical triples composed of three stellar-mass compact objects (e.g., Antonini et al. 2017), neglected in this study, may significantly affect the e distribution. We also have neglected other processes including the formation and evolution of compact objects (and their binaries) other than BHs, and the possible presence of massive perturbers (Deme et al. 2020), which may affect various properties of mergers. Also, BS interactions for nearly 2D cases need to be elucidated using N-body simulations. These effects will be investigated in future work (see also Table 3).

This work is financially supported by the Grants-in-Aid for Basic Research by the Ministry of Education, Science and Culture of Japan (HT:17H01102, 17H06360, KO:17H02869, 17H01102, 17H06360). Z.H. acknowledges support from NASA grant NNX15AB19G and NSF grants AST-1715661 and AST-2006176. Simulations and analyses were carried out on Cray XC50 and computers at the Center for Computational Astrophysics, National Astronomical Observatory of Japan. This project has received funding from the European Research Council (ERC) under the European Union's Horizon 2020 research and innovation program ERC-2014-STG under grant agreement No. 638435 (GalNUC) to BK.

Appendix A
Alternative Models

Here we present the dependence of the eccentricity distribution using a total of 26 different models, listed in Table 4. Figure 3 shows the e distributions for models M1, M2, M5–M9, M12–M16, and M18–M22. Panels (a)–(b) show the dependence on $N_{\rm int}$ when BS interactions occur in isotropic-3D,

Table 4
Same with Table 2, but Results for All Models

Input		Output							
Model	Parameter	$f_{\rm noGWC}$	$f_{\rm GWSS}$	$f_{\rm GWBS}$	$f_{\rm e,0-003}$	$f_{\rm e,003-03}$	$f_{\rm e,03-09}$	$f_{\rm e,09-1}$	$N_{\rm mer}$
M1	Fiducial	0.93	0.02	0.05	0.86	0.065	0.022	0.057	1.1×10^{3}
M2	BS in $2\rightarrow3$D	0.14	3×10^{-3}	0.86	0.25	0.082	0.20	0.47	2.3×10^{3}
M3	No BS	0.46	0.54	0	0.46	0.092	0.26	0.19	9.0×10^{2}
M4	$N_{\rm BH,ini}=6000$, $\beta_{\rm v}=1$	0.55	0.38	0.08	0.54	0.27	0.048	0.15	1.3×10^{2}
M5	$N_{\rm int}=10$	0.96	5×10^{-3}	0.03	0.85	0.10	0.0084	0.043	1.1×10^{3}
M6	BS in 2D	0.25	0.02	0.73	0.25	0.10	0.19	0.46	3.1×10^{3}
M7	BS in 2D, $N_{\rm int}=10$	0.49	0.01	0.50	0.41	0.13	0.13	0.34	2.8×10^{3}
M8	BS in $2\rightarrow3$D, $N_{\rm int}=10$	0.27	2×10^{-3}	0.73	0.38	0.070	0.12	0.43	1.8×10^{3}
M9	BS in $2\rightarrow3$D, $N_{\rm int}=3$	0.66	1×10^{-3}	0.33	0.67	0.053	0.065	0.21	1.3×10^{3}
M10	BS in $2\rightarrow3$D, $N_{\rm int}=1$	0.85	0.02	0.13	0.82	0.060	0.022	0.099	1.1×10^{3}
M11	No gas torque on e	0.90	0.02	0.08	0.83	0.064	0.015	0.090	1.2×10^{3}
M12	No gas migration	0.95	1×10^{-3}	0.05	0.92	0.034	0.0099	0.038	2.8×10^{2}
M13	No gas hardening	0.84	0.040	0.12	0.76	0.071	0.067	0.098	1.1×10^{3}
M14	$\dot{M}_{\rm out}=\dot{M}_{\rm Edd}$	0.86	0.01	0.12	0.78	0.086	0.020	0.12	1.1×10^{3}
M15	$r_{\rm out,BH}=0.3$ pc	0.83	0.08	0.08	0.74	0.10	0.034	0.12	4.8×10^{2}
M16	$M_{\rm SMBH}=4\times10^{7}M_{\odot}$	0.87	0.04	0.09	0.78	0.11	0.035	0.076	1.1×10^{3}
M17	$\Gamma_{\rm Edd,cir}=10$	0.92	0.01	0.07	0.86	0.066	0.030	0.048	1.1×10^{3}
M18	$\beta_{\rm v}=1$	0.79	0.15	0.06	0.70	0.058	0.098	0.15	2.9×10^{2}
M19	$\delta_{\rm IMF}=1.7$	0.92	7×10^{-4}	0.08	0.84	0.073	0.018	0.072	4.5×10^{3}
M20	$M_{\rm star,3pc}=3\times10^{6}M_{\odot}$	0.90	0.03	0.07	0.81	0.075	0.023	0.094	3.5×10^{2}
M21	$\gamma_{\rho}=1.5$	0.87	0.03	0.10	0.78	0.072	0.060	0.089	8.5×10^{2}
M22	$3\times m_{1g}$	0.94	2×10^{-3}	0.06	0.89	0.051	0.022	0.043	1.5×10^{3}
M23	$N_{\rm BH,ini}=2000$	0.85	0.10	0.06	0.69	0.13	0.075	0.10	2.2×10^{2}
M24	$N_{\rm BH,ini}=2000$, $\beta_{\rm v}=1$	0.28	0.72	0	0.26	0.54	0.065	0.14	56
M25	$f_{\rm pre}=0.7$	0.91	5×10^{-3}	0.08	0.87	0.050	0.019	0.065	1.3×10^{3}
M26	No exchange in BS	0.95	9×10^{-3}	0.04	0.88	0.066	0.025	0.028	3.7×10^{3}

Note. "BS in 2D" represents the model in which BS interactions occur in 2D. "No BS" represents the model in which BS interactions do not operate. "No gas torque on ecc," "No gas hardening," and "No gas migration," respectively, represent the models in which the gaseous torques are neglected with respect to the evolution of e, the binary semimajor axis, and the radial position of the binary center of mass within the AGN disk. "$3\times m_{1g}$" represents the model in which initial BH masses are multiplied by 3. "No exchange in BS" represents the model in which the binary components are not exchanged during BS interactions.

2D, or $2\rightarrow3$D directions (Section 2.5). When BS interactions occur in isotropic-2D directions, we assume that e follows $f_{\rm 2D}(e)$ after BS interactions if both the binary and the third body are in the AGN disk and $f_{\rm 3D}(e)$ otherwise (models M6 and M7). The panels demonstrate that $N_{\rm int}$ significantly influences $f_{\rm GWBS}$ and the e distribution of mergers (models M1, M2, M5–M9). Here, the fiducial value of $N_{\rm int}\sim20$ is motivated by numerical simulations in Samsing et al. (2014) and Samsing et al. (2020a) for equal-mass and isotropic-3D or 2D cases.

The eccentricity distributions for models with $2\rightarrow3$D and 2D BS interactions are similar with each other (green lines in panels (a) and black lines in panels (b)), while $\chi_{\rm p}$ is always zero for 2D cases as we assume that binary orbital angular momentum directions are not randomized after 2D BS interactions. If this assumption is reasonable, models with pure 2D BS interactions may be difficult to produce GW190521-like merger, which has nonzero $\chi_{\rm p}$. As models with 2D BS interactions may be already excluded, we present the model with $2\rightarrow3$D BS interactions in the main text, which is also possible to be occurring in AGN disks as discussed in Section 2.5.

We here discuss the feasibility of 2D (and $2\rightarrow3$D) interactions. If the velocities of BHs are damped due to interactions with gas before BS interactions, the interactions could be confined to a 2D plane. This is because the velocity of BHs perpendicular to the AGN disk v_z is $\sim0.01\,{\rm km\,s^{-1}}$ at $r\sim$ pc after the velocity damping (see Figure 5 in Paper I), which is much smaller than

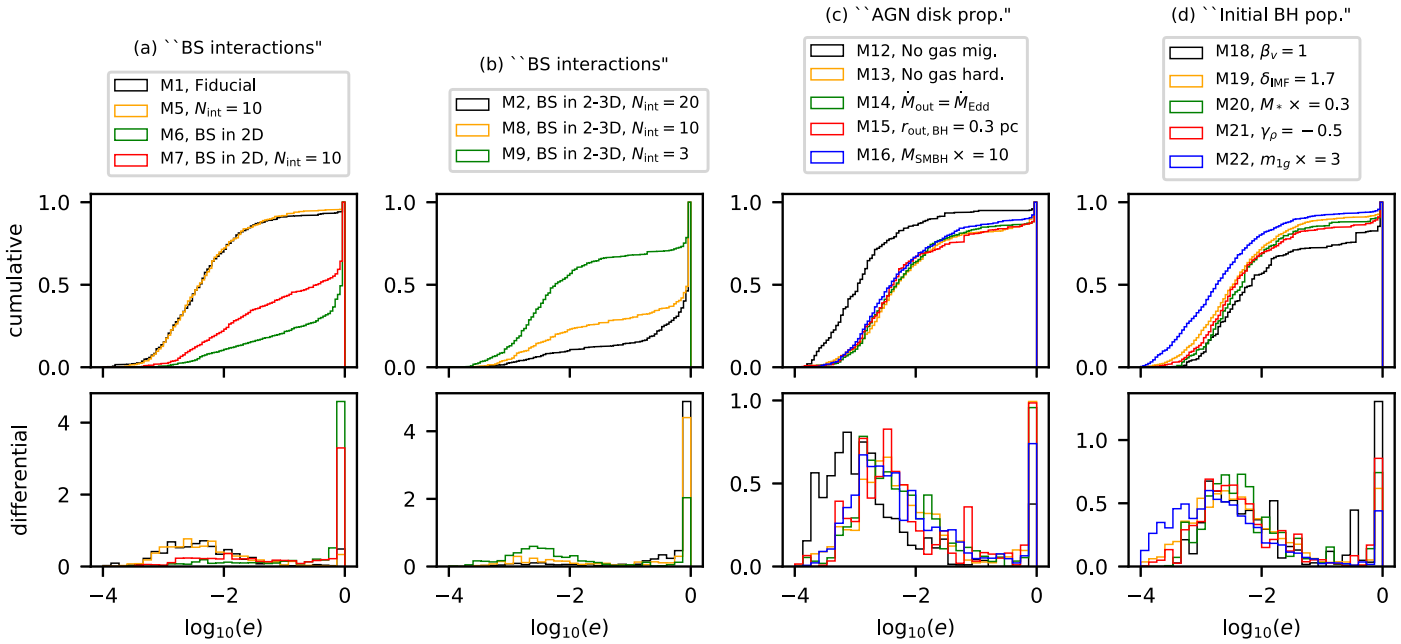

Figure 3. The cumulative (top row) and differential (bottom row) detection rate distributions for the eccentricity at 10 HZ among all merging binaries for models M1, M2, M5–M9, M12–M16, and M18–M22. Different colors and rows present the distributions for different variations of the models, as labeled on the upper legends and listed in Table 2.

$v_{\rm kep}\sim 100\ {\rm km\ s^{-1}}(r/{\rm pc})^{-1/2}(M_{\rm SMBH}/4\times10^6\,M_\odot)^{1/2}$. Referring to these values, the typical orbital elevation of BHs after damping is approximately $\sim(v_z/v_{\rm kep})r\sim10^{-4}r$ at $r\sim$ pc and the Hill radius of BHs with $\sim10\,M_\odot$ is $\sim10^{-2}r$. Thus, the inclination of orbits passing inside the Hill radius is $\sim10^{-2}$, justifying the assumption that interactions might occur in a 2D plane, and our models with 2D or 2D $\rightarrow$ 3D interactions. On the other hand, around $r\sim0.01$ pc, BS interactions occur soon after the binary is captured to the AGN disk (Figure 5 in Paper I), whose timescale is much shorter than the migration timescale ($t_{\rm mig}\gtrsim0.3$ Myr, Figure 10 of Paper I). This implies that interacting objects orbit in similar annuli without migrating motion, and interactions occur while their velocities are still being damped. In this case, the directions of interactions likely become 3D. We conclude that the inclination angles during the BS interactions are roughly confined in a 2D plane in the outer regions of the AGN disk, while they approach a 3D distribution around $r\sim0.01$ pc, where the BH density is high. However, as also mentioned in the main text, possible inhomogeneities/warps of the AGN disk, ignored in our model, may weaken or diminish any alignment and suppress 2D (or 2D $\rightarrow$ 3D) interactions. As there are several uncertainties regarding this issue, further investigations would be required to understand this issue more thoroughly.

We also study several parameters related to the properties of the AGN disk in panels (c) (models M12–M17), the initial BH population in panels (d) (models M18–M24), and gaseous torque (model M11). We find that the e distribution is less affected by many parameters and processes, such as torque from circumbinary disks (model M11), hardening due to gaseous processes (model M13), the accretion rate from outer regions (model M14), the size of AGN disks (model M15), the mass of the SMBH (model M16), the accretion rate onto stellar-mass BHs (model M17), the slope of the initial mass function (model M19), the total mass of stars (model M20), or the slope of the initial radial distribution of BHs (model M21). Indeed, the e distribution is determined almost entirely by the rate of BS interactions and GWC binary formation. The important process regulating the rates is the migration of BHs to the dense inner regions where interactions are frequent.

On the other hand, $e_{10\,\rm Hz}$ is confined to low values when radial migration does not operate (model M12, black lines in panels (c) of Figure 3) or if the initial BH masses are 3$\times$ larger (model M22, blue lines in panels (d) of Figure 3). The frequency of BS interactions is influenced by these changes as follows. When radial migration does not operate (model M12), BS interactions become less frequent as migration enhances the BH density in gap-forming inner regions where migration slows down and BHs accumulate (e.g., Paper I). Also, in the outer regions, it takes longer for binaries kicked by BS interactions to be re-captured to the AGN disk. Then a longer time is available to the binaries to merge by GW emission, reducing the eccentricity at merger. Similar effects are expected when the initial BH masses are multiplied by 3 (model M22). In this model, massive BHs open gaps in regions further out, and mergers occur at $r\sim0.003$–3 pc in model M22, while those in the fiducial model are limited to $r\sim0.003$–0.03 pc. As these parameters affect the eccentricity distribution at low e, these variations are expected to be constrained by LISA. Overall, capture of BHs into the AGN disk and migration to gap-forming inner regions increases the rate of BS interactions, which increases the typical values of $e_{10\rm Hz}$, in addition to prescriptions for BS interactions. On the other hand, the $e_{10\rm Hz}$ distribution is less affected by other processes.

Also, the detection fraction of mergers among SS–GWC binaries ($f_{\rm GWSS}$) increases as the BH density in the AGN disk is reduced (models M4, M18, M23, and M24). When the BH density in the AGN disk is low, BS interactions are infrequent, and then, BHs can easily migrate to the inner AGN disk where SS–GWC binary formation is efficient as discussed in the main text. It may be possible to constrain the efficiency of migration of BHs in the AGN disk by measuring $f_{\rm GWSS}$ by LIGO/Virgo/KAGRA.

When the exchange at BS interactions is neglected (model M26 or all models in Paper I/Paper II), light BHs

easily reside in binaries and merge. As the energy required to be extracted from the binary to merge is smaller for lighter binaries, the number of mergers among non-GWC binaries is enhanced by ignoring the exchange (Table 3).

ORCID iDs

Bence Kocsis https://orcid.org/0000-0002-4865-7517
Zoltán Haiman https://orcid.org/0000-0003-3633-5403
Imre Bartos https://orcid.org/0000-0001-5607-3637
Kazuyuki Omukai https://orcid.org/0000-0001-5922-180X
Johan Samsing https://orcid.org/0000-0003-0607-8741

References

Abbott, B. P., Abbott, R., Abbott, T. D., et al. 2019a, ApJ, 883, 149
Abbott, B. P., Abbott, R., Abbott, T. D., et al. 2019b, PhRvX, 9, 031040
Abbott, R., Abbott, T. D., Abraham, S., et al. 2020a, arXiv:2009.01075
Abbott, R., Abbott, T. D., Abraham, S., et al. 2020b, ApJL, 900, L13
Abbott, R., Abbott, T. D., Abraham, S., et al. 2020c, arXiv:2004.08342
Abbott, R., Abbott, T. D., Abraham, S., et al. 2020d, ApJL, 896, L44
Antonini, F., & Perets, H. B. 2012, ApJ, 757, 27
Antonini, F., Toonen, S., & Hamers, A. S. 2017, ApJ, 841, 77
Arca-Sedda, M., Li, G., & Kocsis, B. 2018, arXiv:1805.06458
Bartos, I., Kocsis, B., Haiman, Z., & Márka, S. 2017, ApJ, 835, 165
Breivik, K., Rodriguez, C. L., Larson, S. L., Kalogera, V., & Rasio, F. A. 2016, ApJL, 830, L18
Deme, B., Meiron, Y., & Kocsis, B. 2020, ApJ, 892, 130
Farmer, R., Renzo, M., de Mink, S. E., Marchant, P., & Justham, S. 2019, ApJ, 887, 53
Fragione, G., & Bromberg, O. 2019, MNRAS, 488, 4370
Fragione, G., Grishin, E., Leigh, N. W. C., Perets, H. B., & Perna, R. 2019, MNRAS, 488, 47
Fuller, J., & Ma, L. 2019, ApJL, 881, L1
Gayathri, V., Healy, J., Lange, J., et al. 2020, arXiv:2009.05461
Gondán, L., & Kocsis, B. 2019, ApJ, 871, 178
Gondán, L., & Kocsis, B. 2020, arXiv:2011.02507
Gondán, L., Kocsis, B., Raffai, P., & Frei, Z. 2018, ApJ, 860, 5
Graham, M. J., Ford, K. E. S., McKernan, B., et al. 2020, PhRvL, 124, 251102
Heggie, D. C. 1975, MNRAS, 173, 729
Huerta, E. A., & Brown, D. A. 2013, PhRvD, 87, 127501
Kocsis, B., Gáspár, M. E., & Márka, S. 2006, ApJ, 648, 411
Leigh, N. W. C., Geller, A. M., McKernan, B., et al. 2018, MNRAS, 474, 5672
Lower, M. E., Thrane, E., Lasky, P. D., & Smith, R. 2018, PhRvD, 98, 083028
Lubow, S. H., Seibert, M., & Artymowicz, P. 1999, ApJ, 526, 1001
Martinez, M. A. S., Fragione, G., Kremer, K., et al. 2020, ApJ, 903, 67
McKernan, B., Ford, K. E. S., Bartos, I., et al. 2019, ApJL, 884, L50
McKernan, B., Ford, K. E. S., Bellovary, J., et al. 2018, ApJ, 866, 66
Muñoz, D. J., Miranda, R., & Lai, D. 2019, ApJ, 871, 84
Nishizawa, A., Berti, E., Klein, A., & Sesana, A. 2016, PhRvD, 94, 064020
O'Leary, R. M., Kocsis, B., & Loeb, A. 2009, MNRAS, 395, 2127
Peters, P. C. 1964, PhRv, 136, 1224
Rasskazov, A., & Kocsis, B. 2019, ApJ, 881, 20
Rodriguez, C. L., Amaro-Seoane, P., Chatterjee, S., et al. 2018, PhRvD, 98, 123005
Romero-Shaw, I. M., Lasky, P. D., & Thrane, E. 2019, arXiv:1909.05466
Romero-Shaw, I. M., Lasky, P. D., Thrane, E., & Calderon Bustillo, J. 2020, arXiv:2009.04771
Samsing, J. 2018, PhRvD, 97, 103014
Samsing, J., Bartos, I., D'Orazio, D. J., et al. 2020a, arXiv:2010.09765
Samsing, J., & D'Orazio, D. J. 2018, MNRAS, 481, 5445
Samsing, J., D'Orazio, D. J., Kremer, K., Rodriguez, C. L., & Askar, A. 2020b, PhRvD, 101, 123010
Samsing, J., & Ilan, T. 2019, MNRAS, 482, 30
Samsing, J., MacLeod, M., & Ramirez-Ruiz, E. 2014, ApJ, 784, 71
Sigurdsson, S., & Phinney, E. S. 1993, ApJ, 415, 631
Silsbee, K., & Tremaine, S. 2017, ApJ, 836, 39
Stone, N. C., Metzger, B. D., & Haiman, Z. 2017, MNRAS, 464, 946
Szolgyen, A., & Kocsis, B. 2018, PhRvL, 121, 101101
Tagawa, H., Haiman, Z., Bartos, I., & Kocsis, B. 2020a, ApJ, 899, 26
Tagawa, H., Haiman, Z., & Kocsis, B. 2020b, ApJ, 898, 25
Thompson, T. A., Quataert, E., & Murray, N. 2005, ApJ, 630, 167
Valtonen, M., & Karttunen, H. 2006, The Three-body Problem (Cambridge: Cambridge Univ. Press)
Wen, L. 2003, ApJ, 598, 419
Yang, Y., Bartos, I., Gayathri, V., et al. 2019, PhRvL, 123, 181101
Yang, Y., Gayathri, V., Bartos, I., et al. 2020, arXiv:2007.04781
Zackay, B., Dai, L., Venumadhav, T., Roulet, J., & Zaldarriaga, M. 2019, arXiv:1910.09528
Zevin, M., Samsing, J., Rodriguez, C., Haster, C.-J., & Ramirez-Ruiz, E. 2019, ApJ, 871, 91
Zrake, J., Tiede, C., MacFadyen, A., & Haiman, Z. 2020, arXiv:2010.09707